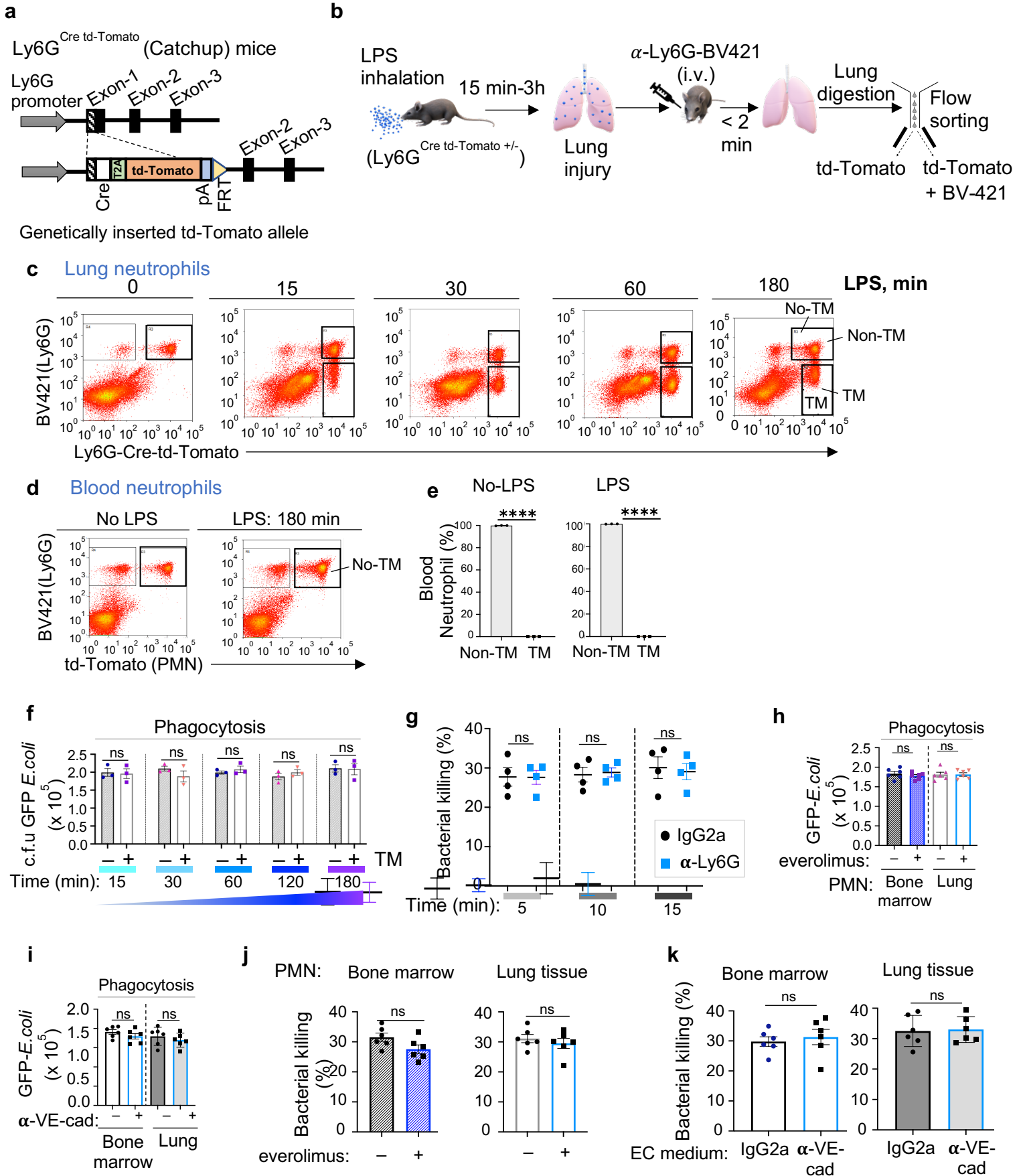


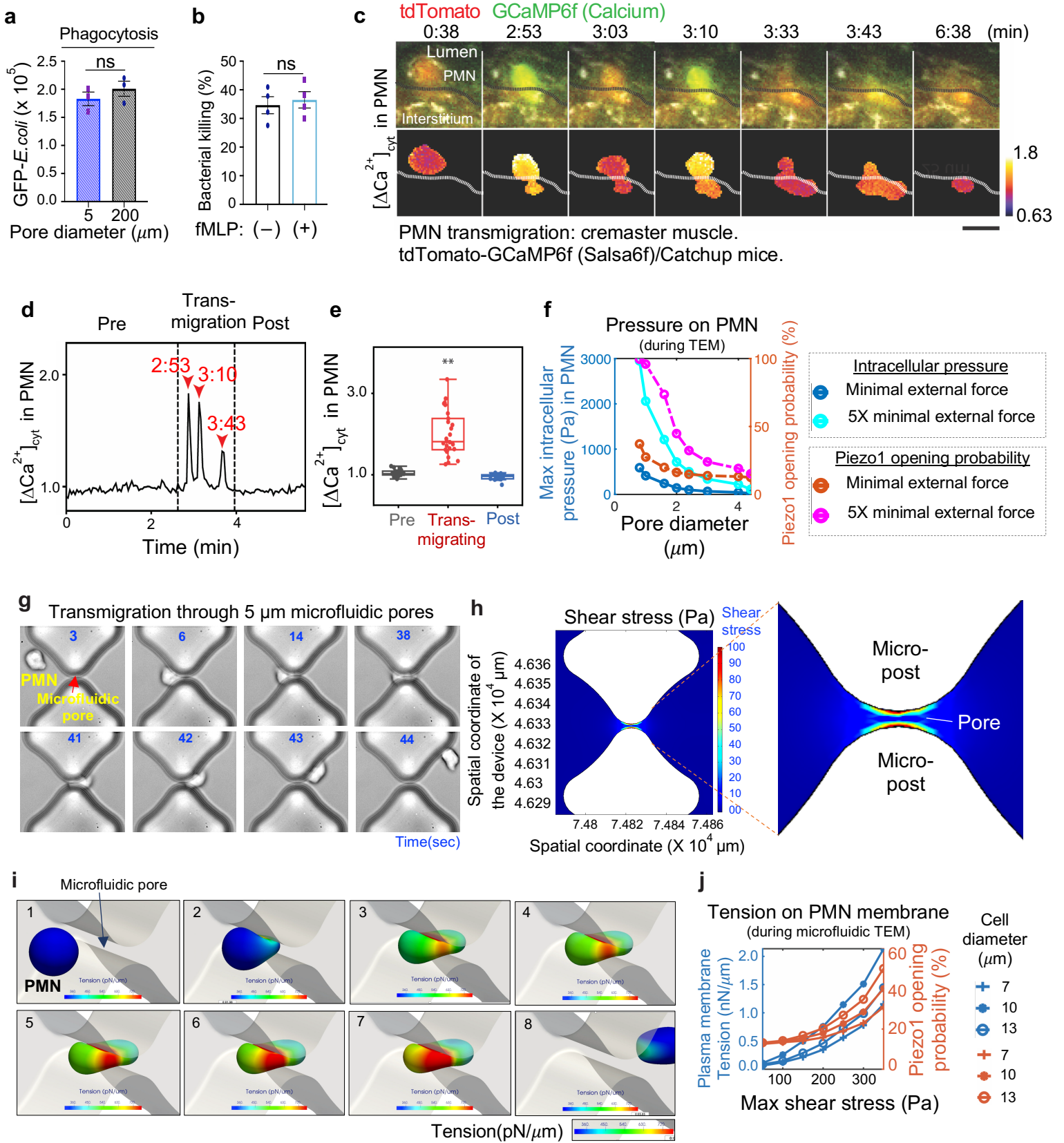
# Supplementary Figures

# Supplementary Figure 1



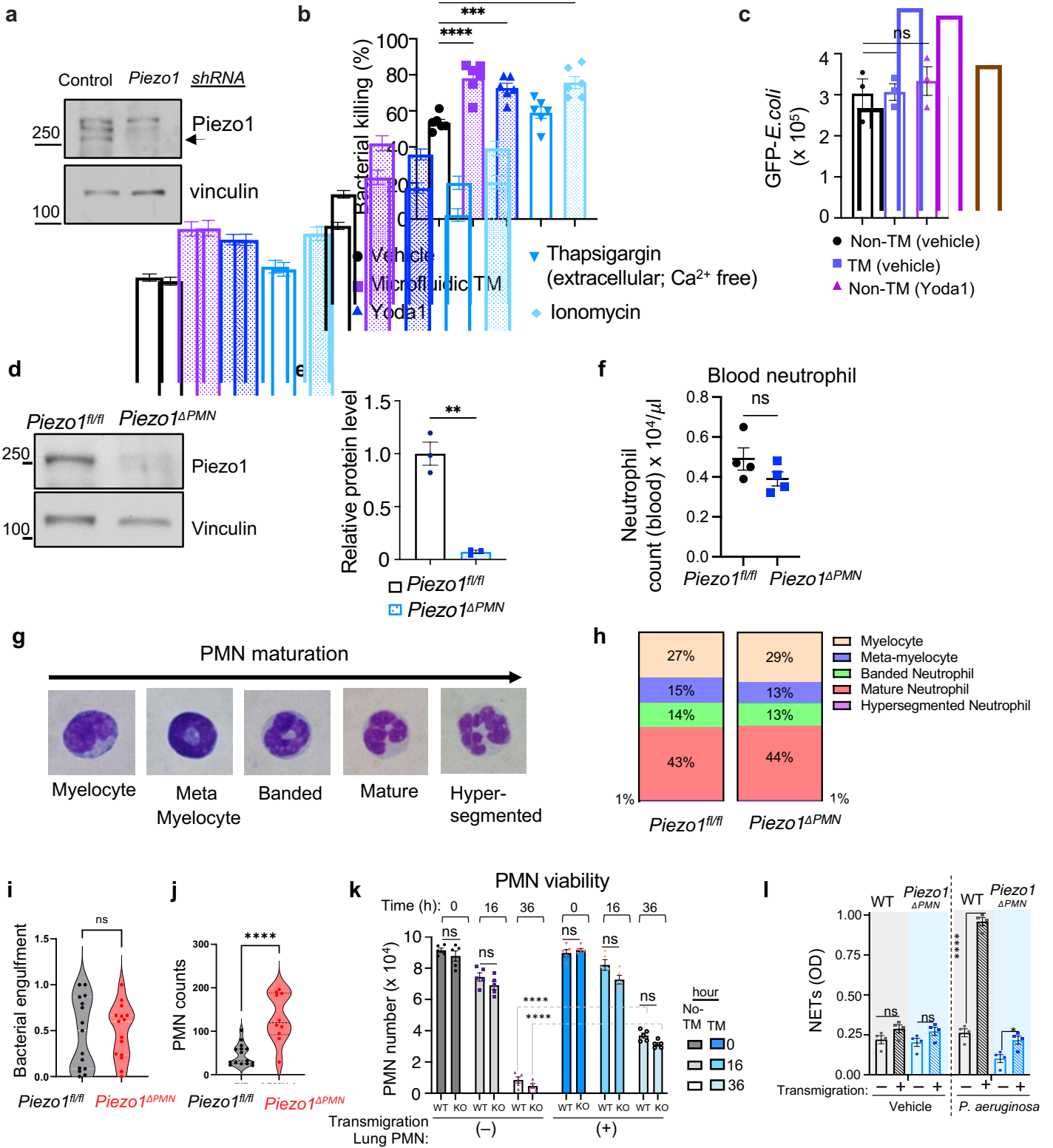
**Supplement Figure 1 – related to Figure 1. Transmigrated PMN demonstrate enhanced antimicrobial function.** **a.** Schematic demonstrating td-Tomato and Cre transgene insert into exon1 locus of Ly6G gene to produce heterozygous Catchup mice (Ly6G<sup>Cre td-Tomato +/-</sup>) expressing both td-Tomato and Cre in PMN. These mice were used to distinguish non-transmigrated and transmigrated lung tissue PMN. **b.** Schematic showing the time-course experiments in **Figure 1b-e** in which PMN transmigration was induced with 5mg/ml insufflated LPS for the indicated times. **c-e.** FACS analysis demonstrates non-transmigrated (td-Tomato and anti-Ly6G-BV421 double-positive) and transmigrated (td-tomato-positive) lung PMN from control (-LPS) and LPS-challenged (+LPS) mice at indicated times post-exposure to 5mg/ml insufflated LPS. Transmigrated (TM) PMN appear in the bottom right quadrant. **c.** FACS profiles of lung and **d.** peripheral blood PMN and **e.** quantification of data in **d.** All peripheral blood PMN were double-positive for td-Tomato and Ly6G-BV-421 in both naïve and LPS-challenged mice. Data are obtained from 3 mice per group from 3 independent experiments. **f.** GFP-*E.coli* phagocytosis by transmigrated (+) and non-transmigrated (-) lung PMN at indicated times post-exposure to 5mg/ml insufflated LPS as in **Figure 1e**. **g.** A short incubation of bone-marrow murine PMN with  $\alpha$ -Ly6G or matched control antibodies had no effect on bacterial killing; control conditions for the **Figure 1e**. Data are presented as 4 samples per group from 2 independent experiments. **h.** GFP-*E.coli* phagocytosis by transmigrated (+) and non-transmigrated (-) lung PMN isolated from transgenic mice expressing engineered VE-cadherin-FK506 and VE-PTP-FRB fusion proteins or bone-marrow PMN with and without treatment with everolimus as in **Figure 1h**. **i.** GFP-*E.coli* phagocytosis by transmigrated (+) and non-transmigrated (-) lung PMN isolated from C57B6 mice treated with isotype-matched antibody as well as functional blocking anti-VE-cadherin antibody as in **Figure 1j**. **j-k.** Treatment of bone marrow or lung tissue murine PMN with everolimus (**j**) or with supernatant of endothelial monolayers incubated with anti-VE-cadherin or match control antibodies for 4h (**k**) did not alter GFP-*E.coli* killing *ex vivo*; control conditions for **Figure 1h, j**. Data are obtained from 4 independent experiments.

## Supplementary Figure 2



**Supplement Figure 2 – related to Figure 2 & 3 (a-h). PMN transmigration does not alter phagocytosis. a.** GFP-*E.coli* phagocytosis by bone marrow murine PMN perfused through the 5 $\mu$ m or 200 $\mu$ m diameter pores of the microfluidic system as in **Figure 2b. b.** Exposure of bone marrow murine PMN grown in suspension to 1 $\mu$ M fMLP had no effect on GFP-*E.coli* killing *ex vivo*; control conditions for **Figure 2e**. Data are obtained from 4 independent experiments. **c-j. Activation of calcium influx in PMN during transendothelial migration in cremaster muscle micro-vessel and microfluidic system. c-e.** Ca<sup>2+</sup> influx in PMN transmigrating in cremaster muscle micro-vessel. **c.** Ca<sup>2+</sup> transients in PMN determined by live intravital imaging of calcium indicator GCaMP6f before, during, and after transmigration of peripheral blood PMN across endothelial AJs of vessels of cremaster muscle. The color gradient shows blue as the lowest and yellow as highest increase in cytosolic [Ca<sup>2+</sup>] as indicated. The dotted line shows the intimal endothelium. Time in min and sec. Scale bar, 10 $\mu$ m. Realtime video is provided as supplementary **Video S4. d.** Graph showing changes in cytosolic [Ca<sup>2+</sup>] during PMN transmigration in **c.** **e.** Quantitation of Ca<sup>2+</sup> peaks normalized to baseline fluorescence prior to transmigration. Data are obtained from 3 mice. **f.** Dependence of membrane pressure and the open probability of Piezo1 channel on pore diameter and applied external forces. Results are derived from the computational model described in methods section. **g.** Time-lapse images obtained at 30,000 frame/sec show PMN passing through 5  $\mu$ m pore of the microfluidic system. Realtime video is provided as supplementary **Video S3. h.** Quantification of fluid shear stress in the microfluidic system at flow of 10  $\mu$ l/min. **i.** Predicted changes in PMN plasma membrane tension during passage of PMN through a pore of microfluidic system using the described computational model. Video is provided as supplementary **Video S5**. The color map shows the PMN membrane tension and pressure experienced on the membrane. **j.** Membrane tension and Piezo1 activation probability as a function of maximum shear stress and cell diameter in the microfluidic system predicted from **i**.

### Supplementary Figure 3

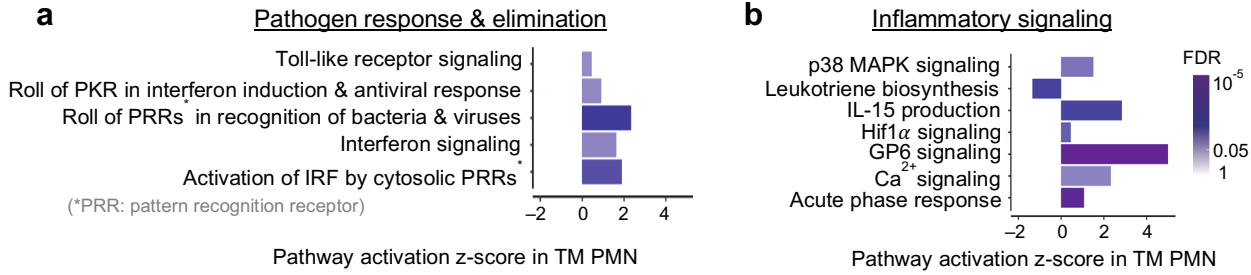


**Supplement Figure 3 – related to Figure 3 (i-k) & 4. Characterization of PMN genetically deleted of Piezo1.**

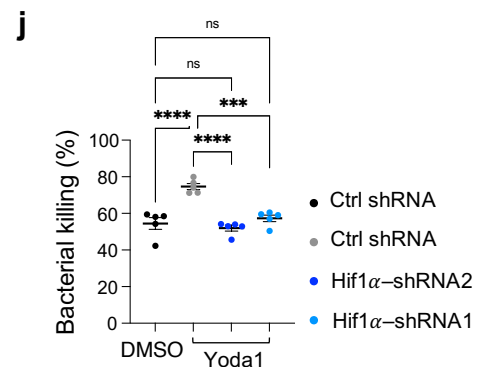
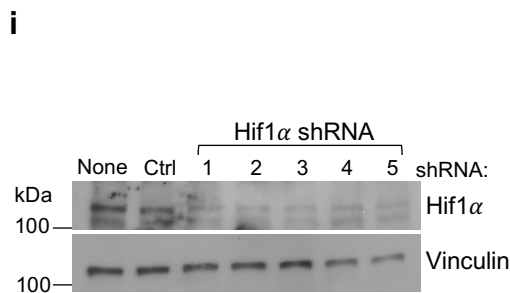
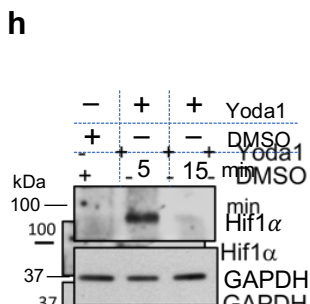
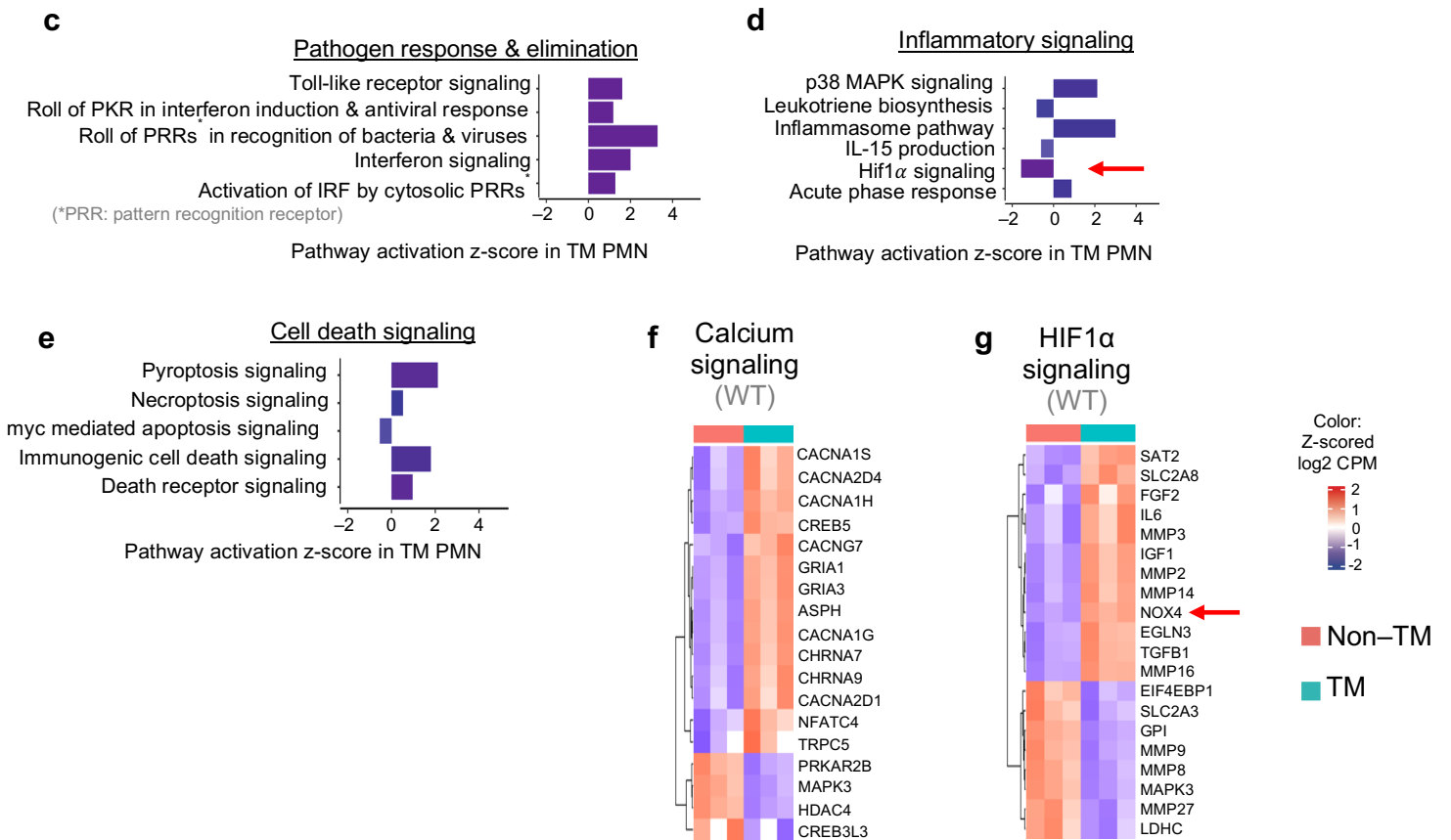
**a.** Western blot analysis of Piezo1 expression in HL-60 derived PMN that were transduced with lentiviral particles carrying control or targeting sequence of Piezo1 shRNA. Vinculin was used as a loading control. **b.** Bactericidal activity of bone marrow murine PMN treated with 10 $\mu$ M of the inhibitor of sarco-endoplasmic reticulum Ca<sup>2+</sup> ATPase, thapsigargin, in the absence of extracellular Ca<sup>2+</sup> or treated with ionomycin or Yoda1 in presence of extracellular Ca<sup>2+</sup>. The effects of these treatments were compared to effects of PMN transmigrated through 5 $\mu$ m pores of microfluidic system. Data are presented from 6 independent experiments. **c.** GFP-*E.coli* phagocytosis by human PMN grown in suspension and treated with vehicle or Yoda1 or by PMN post-transmigration through 5 $\mu$ m pores of microfluidic system. Results are obtained from 3 healthy human subjects from 3 independent experiments. **d-e.** Western blot analysis of Piezo1 expression in bone marrow PMN isolated from control *Piezo1<sup>fl/fl</sup>* and *Piezo1 <sup>$\Delta$ PMN</sup>* mice.  $\beta$ -actin was used as a loading control and quantification of data in **e**. Data are presented as 3 mice per group. **f.** Piezo1 deficiency in PMN did not alter the number of PMN in peripheral blood as assessed using automated counter. Data were obtained from 4 mice per group. **g-h.** Piezo1 deficiency did not alter maturation of PMN. PMN maturation stages in bone marrow of control and *Piezo1 <sup>$\Delta$ PMN</sup>* mice analyzed using nuclear shapes. Representative images of H&E staining from 3 independent experiments (**g**) and quantification of myelocytes, meta-myelocytes, banded PMN, mature PMN, and hyper-segmented PMN as indicated (**h**). n=141-150 total number cells for each of the two groups. Data are presented for 3 independent experiments. **i-l. Role of Piezo1 on PMN function post-transendothelial migration.** **i-j.** Number of PMN containing GFP-*Pseudomonas aeruginosa* (**i**) and total number of PMN (**j**) in lung tissue of control and *Piezo1 <sup>$\Delta$ PMN</sup>* mutant mice challenged with 10<sup>6</sup> cfu bacteria per mouse for 12h; data corresponding to **Figure 4h**. **k-l.** PMN viability and NETosis post-transmigration. Transmigrated and non-transmigrated lung PMN were isolated from control and *Piezo1 <sup>$\Delta$ PMN</sup>* mice and cultured *ex vivo* for indicated times to assess their viability (**k**) or were exposed to 10<sup>6</sup> cfu bacteria for 1h to assess NET formation (**l**). **k.** Viability of transmigrated lung tissue PMN cultured *ex vivo* was significantly greater than viability of non-transmigrated PMN at 36h but not at the earlier time points. Piezo1 deficiency did not alter PMN viability of transmigrated PMN. Data were obtained from 3 mice per group. **l.** Transmigrated lung PMN exhibited increased formation of NETs upon exposure to GFP-*Pseudomonas aeruginosa*. Piezo1 deficiency in transmigrated lung PMN prevented NET formation. Data were obtained from 3 mice per group.

# Supplementary Figure 4

## Transcriptomic shifts of transmigrated PMNs in wild-type mice

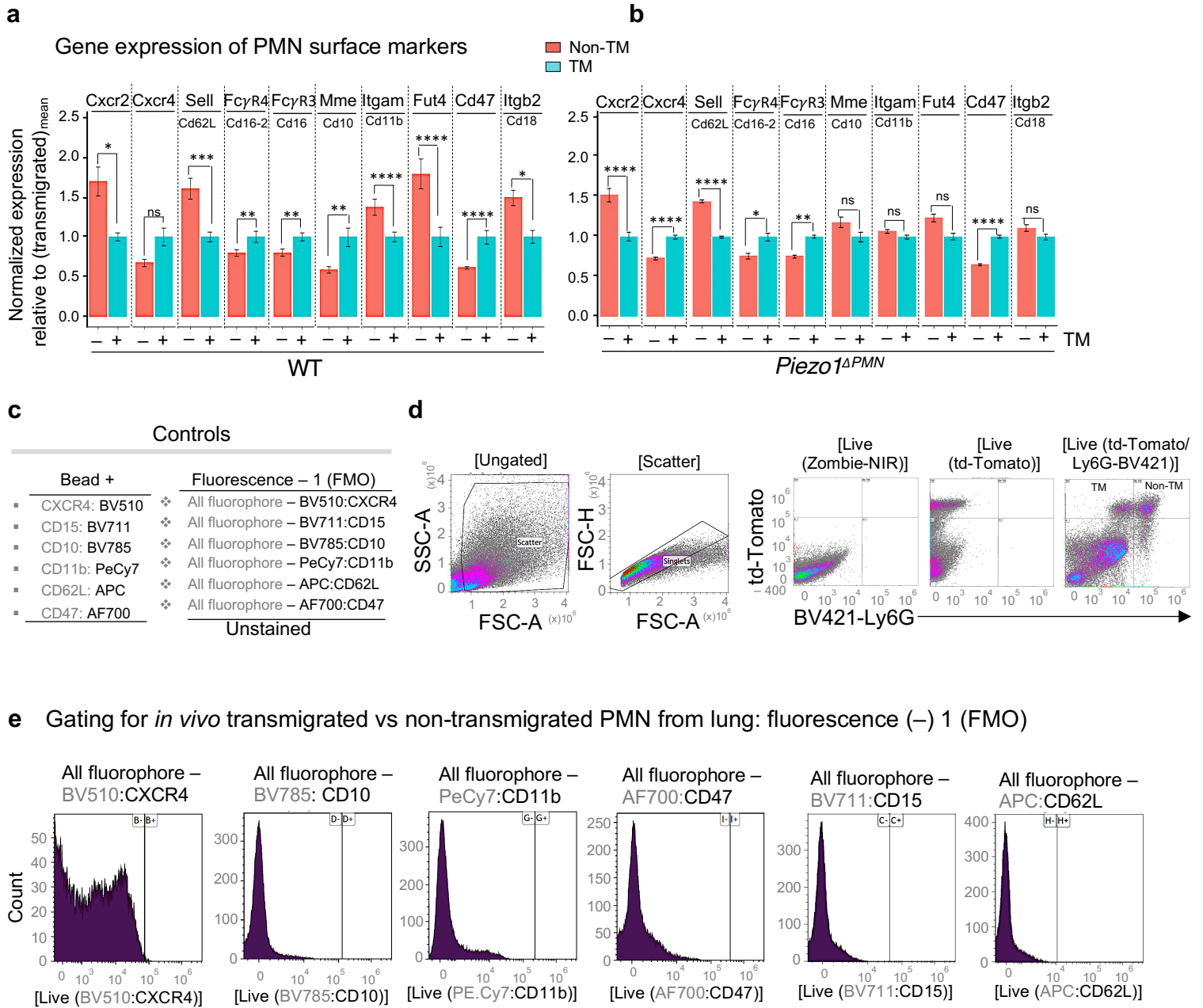


## Transcriptomic shifts of transmigrated PMNs in *Piezo1*<sup>APMN</sup> mice



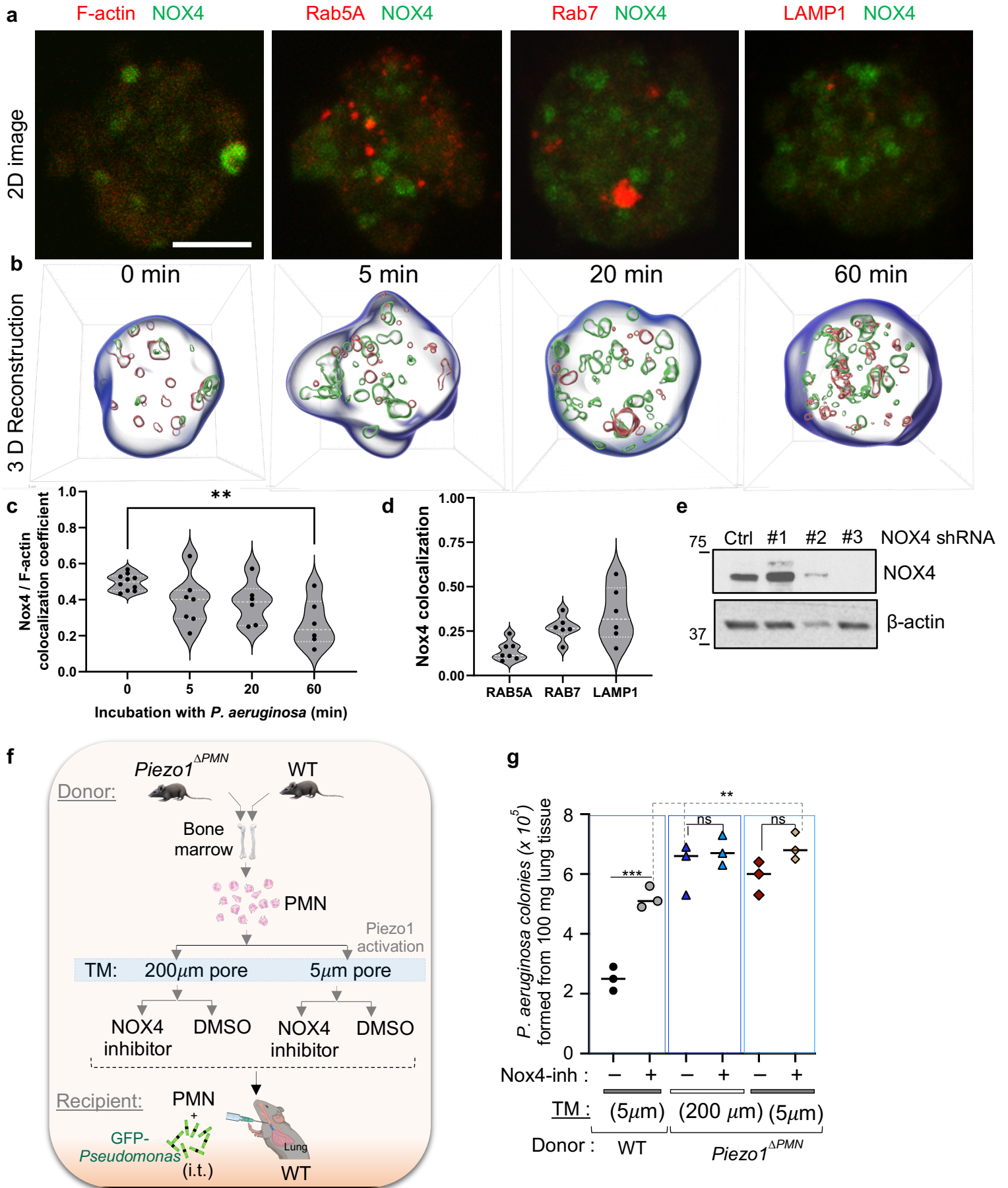
**Supplement Figure 4 – related to Figure 5 (a-g). Piezo1 drives calcium signaling and inflammatory response post-transmigrated PMN. a-e.** Selected pathways significantly enriched among the differentially expressed genes in lung tissue PMN. Analysis compared transmigrated vs non-transmigrated PMN of wild-type and *Piezo1* <sup>$\Delta$ PMN</sup> mice. Individual pathways are grouped according to a broader biological function categorization. Z-scores are computed by Ingenuity Pathway Analysis (IPA) based on comparison between the transmigrated (TM) vs non-transmigrated (non-TM). These data predict activation or repression of the identified pathways; FDRs are t-H corrected p-values used to assess statistical significance. Detailed analysis is included in supplementary **Table1**. **a-b** are pathways enriched in wild-type PMN and **c-e** are pathways enriched in Piezo1 deficient PMN. **f-g.** Heatmaps of differentially expressed genes in “Calcium signaling” and “HIF1 $\alpha$  signaling” pathways in wild-type PMN; z-scored *log*-scaled normalized expression is plotted. **h-j. Piezo1 activation stabilizes Hif1 $\alpha$ .** **h.** Piezo1 activation in human PMN by Yoda1 shows stabilization of Hif1 $\alpha$  within 5m post-treatment. **i.** Western blot shows downregulation of Hif1 $\alpha$  in HL-60 derived PMN infected with lentivirus shRNA targeting Hif1 $\alpha$ . **j.** Lentiviral shRNA-mediated silencing of Hif1 $\alpha$  in differentiated HL-60 derived PMN abrogated bactericidal function in Yoda1 treated cells.

# Supplementary Figure 5



**Supplemental Figure 5 – related to Figure 5 (h).** Transendothelial PMN migration alters expression of cell surface markers. **a, b** Transcriptional changes in cell surface markers of transmigrated vs. non-transmigrated PMN as assessed by RNAseq analysis. Gene expression in counts per million (CPM) presented in linear scale was normalized to mean of the transmigrating PMN group. Of note the genetic ablation of Piezo1 induced upregulation CXCR4 and prevented the upregulation of CD10 in transmigrated PMN. **c.** Spectral flow cytometric analysis of cell surface markers of transmigrated vs. non-transmigrated PMN. List of different controls used in multi-scale flow cytometry experiments. **d.** Gating strategy where cells were gated on scatter properties followed by singlets. Live cells negative for staining with Zombie-NIR were selected for further analyses. td-Tomato and Ly6G double-positive cells were considered non-transmigratory while cells positive for td-Tomato but not stained for Ly6G were considered transmigratory. **e.** Gating strategy using Fluorescence minus one (FMO) controls are shown.

Supplementary Figure 6



**Supplemental Figure 6 – related to Figure 6. Piezo1 upregulates Nox4 expression in transmigrated PMN and activates bactericidal activity.** **a-d.** HL-60 derived PMN expressing NOX4-GFP were exposed to *Pseudomonas aeruginosa* for indicated times and stained for F-actin, Rab5, Rab7, and LAMP1. 2-D projected (**a**) and 3-D reconstructed (**b**) images demonstrate co-localization of NOX4 (green) with indicated markers (red) while the cell surface is blue. Co-localization of NOX4 with F-actin (**c**) and phagosomal, and phagolysosomal markers (**d**). Data are obtained from 2 independent experiments. **e.** Western blot analysis of NOX4 expression in PMN derived from HL-60 cells transduced with lentiviral particles carrying control and 3 different target sequences of NOX4 shRNA.  $\beta$ -actin was used as loading control. **f-g.** Inhibition of NOX4 in Piezo1 deficient PMN had no additive effect on PMN bactericidal function. Bone marrow murine PMN isolated from control or *Piezo1* <sup>$\Delta$ PMN</sup> mice were passed through pore diameters of 5 $\mu$ m or 200 $\mu$ m size microfluidic system and treated with 10 $\mu$ M NOX1 and NOX4 inhibitor, GKT137831, or vehicle control prior i.t. adoptive transfer to lungs of control C57B6 mice challenged with 1x10<sup>6</sup> cfu *Pseudomonas aeruginosa* per mouse. Schematic of the experiment design (**f**) and lung bacteria load (**g**) are shown. Lung tissue was lysed and plated on agar plates. Data are obtained from 3 mice per group.